Universiteit Utrecht

UTRECHT UNIVERSITY

INSTITUTE FOR THEORETICAL PHYSICS

BACHELOR'S THESIS

Dynamical charging and discharging of a capacitive mixing blue engine

Author:
Jurriaan WOUTERS
3837483

Supervisors:
Prof. Dr. René van ROIJ
Dr. Andreas HÄRTEL
Mathijs JANSSEN, M.Sc.
Dr. Sela SAMIN

June 17, 2014

Abstract

Where river water flows in to the sea a lot of entropy is created. A blue engine harvests (blue) energy from this increase in entropy. A device to obtain this energy is a capacitive mixing engine. This engine consists of two supercapacitor-like porous carbon electrodes immersed in water connected to a voltage source. Brogioli designed an equilibrium cycle that extracts this energy by changing the potential and switching the salt and fresh water accordingly. Brogioli calculated that the work per liter of fresh water was 1.6 kJ, which equals the energy of waterfall of 160 m. Because this is an equilibrium cycle, which takes infinitely long, the power output is 0. This Thesis focusses on finding the maximum power output for a Brogioli-like cycle by modeling the dynamics of a pore-reservoir system and using the Poisson and Nernst-Planck equations. Also the equilibrium cycle is calculated and yields a work of 2 kJ per liter of fresh water, which is in agreement with the results of Brogioli. The maximum power output is found around a cycle time of 2.7 μs at 304 W m^{-2}, but highly depends on the flushing times and the length of the pore. If the flushing times are determined the maximum power output can be calculated more accurately.

1

Contents

1 Introduction

In 1954 R.E. Pattle suggested that a huge amount of energy can be harvested at river mouths from the mixing of river and sea water. He calculated that the energy of a river flowing into the sea equals that of a waterfall of 200 m high. He suggested to harvest this energy by using the osmotic properties of sea and river water and he built an apparatus that obtained this energy using membranes to proof this concept [1].

Now, sixty years later harvesting this energy source has become much more realistic. Several different techniques have been developed to harvest this energy. This obtained energy comes from an increase in entropy. Analogue to mixing of two different gases [2], mixing of sea and river water will increase the entropy by huge amount. The ordered salt (sea) water and fresh (river) water turns into a lot of disordered fresh water [3].
The first law of thermodynamics, $dU = TdS - dW$, points out why energy can be harvested in the first place. In this equation U is the internal energy, T is the temperature, S is the entropy and W is the work. If the internal energy does not change and the entropy increases by mixing, then work is done by the system.

One of the methods that uses this increase in entropy is pressure-retarded osmosis (PRO) [3]. A large pressure vessel is filled with horizontal compartments, alternating fresh and salt water. The fresh and salt water compartments are separated by a water permeable membrane. The difference in osmotic pressure, i.e. chemical potential, forces water to flow from the compartments with low salt concentration to the compartments with high concentration. The difference in hydrostatic pressure that results can be used to drive a turbine with a generator.
Another method, reverse electrodialysis (RED), also uses this difference in chemical potential. RED also needs the fact that salt consist of ions (Na^+ and Cl^-) [3]. Again a container is filled with alternating fresh and salt water compartments, but now the membranes separating a salt water compartment from the fresh water are different. The membranes are not permeable by water but by the ions. One is only permeable by the positive ions (the left one) and the other by the negative ions (the right one). Since the system wants to restore the difference in chemical potential, the ions flow from the high to the low salt concentration. The membranes do not allow both ions to flow, so there is a net flow of positive ions in one direction (to the left) and a net flow of negative ions in the other direction (to the right). This gives a charge flow from one to the other (to the left). If the walls are connected by conducting material, global charge neutrality ensures a flow of electrons between the walls to account for the flow of ions. This flow of electrons is due to redox reactions on the walls.

In 2009, Brogioli [4] proposed a completely different method, which is based on capacitive mixing. The idea for this system arose, because new technologies were available to mass produce porous carbon electrodes, vital to this system. A capacitive mixing device has two supercapacitor-like electrodes filled with water and connected to opposing poles of a voltage source. By changing the voltage and mixing the sea and river water in a certain way, energy is retrieved from the system. This is the system that will be investigated in this Thesis. A lot of research has been done on the stationary or equilibrium solutions of this system [4, 5, 6]. Unfortunately, it is not practical to have a system that is constantly in equilibrium, since the power output $\left(\frac{\text{Energy per cycle}}{\text{Time per cycle}} \right)$ will be very low for such a system, because the time of an equilibrium cycle will be very long. Therefore the cycle that does not take infinite time will be investigated. On the other hand, taking shorter times, not every bit of energy is squeezed out of the mixing. This raises a new question: is there a maximum power output for the charging time larger than zero and smaller than infinity? Hence this Thesis will focus on finding maximal power output for a capacitive mixing engine, by investigating the dynamics of this system.

2 Blue engine with capacitive mixing

The capacitive mixing process is essentially adsorbing salt ions from the salt water at low potential and releasing ions into fresh water at high potential. This adsorbing takes place in porous carbon electrodes. Figure 1 shows the electrodes immersed in the electrolyte (water with dissolved salt) connected to a voltage source.
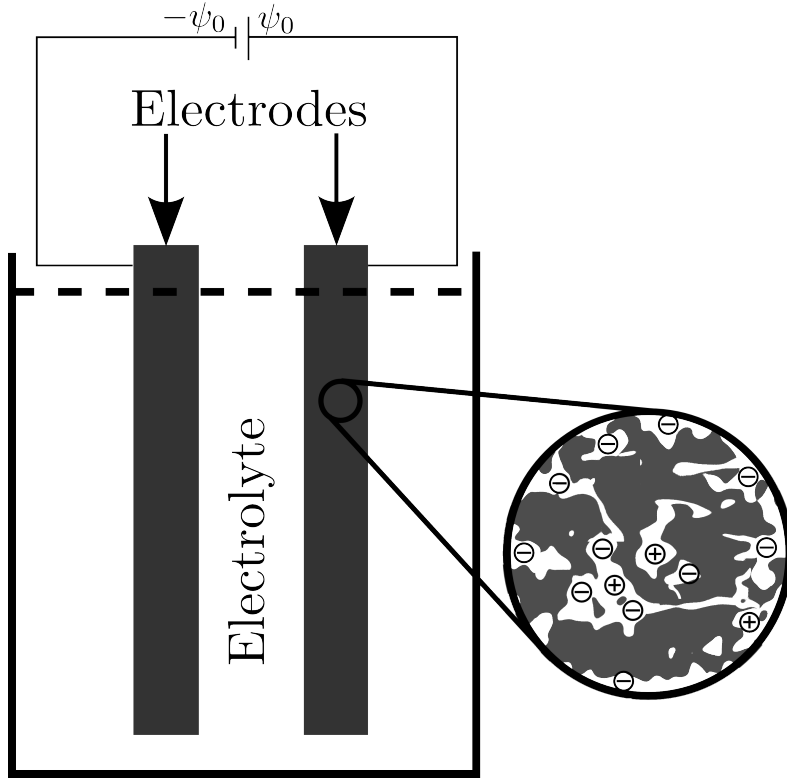
Figure 1: Schematic display of the porous electrodes in electrolyte connected to a voltage source.

The electrodes consist of highly porous activated carbon. The porosity is important, because in this way the electrodes have a large effective surface and therefore a high adsorption of ions. When a potential is applied to an electrode, a double layer forms. In this double layer the ions are adsorbed. Since the double layers form at the surface of the electrode, the adsorption of ions scales linear with surface of the electrode. So the large surface of the porous carbon results in high absorption of ions. The surface of activated porous carbon electrodes is approximately
10^3 m^{2}g^{-1} [7]. The most common electrodes have average pore radius of 1.5 nm [8, 9].
The pores within a porous material are categorised by the International Union of Pure and Applied Chemistry (IUPAC): micropores ($R < 1$ nm), mesopores (1 nm $\leq R < 25$ nm) and macropores ($R \geq 25$ nm), where R is the radius of the pore [10]. The most suitable materials for the blue engine are microporous materials (materials which contain a high percentage micropores), because these materials have the largest surface per gram of carbon and therefore the largest adsorption.

2.1 Previous research

In 2009 Brogioli published the first article that presented a blue engine based on capacitive mixing [4]. He described how energy was obtained from the mixing of salt and fresh water through a cycle analogue to the Stirling heat engine. Figure 2 displays the ABCDA-cycle in the potential-charge ψ-Q representation, Brogioli suggested.
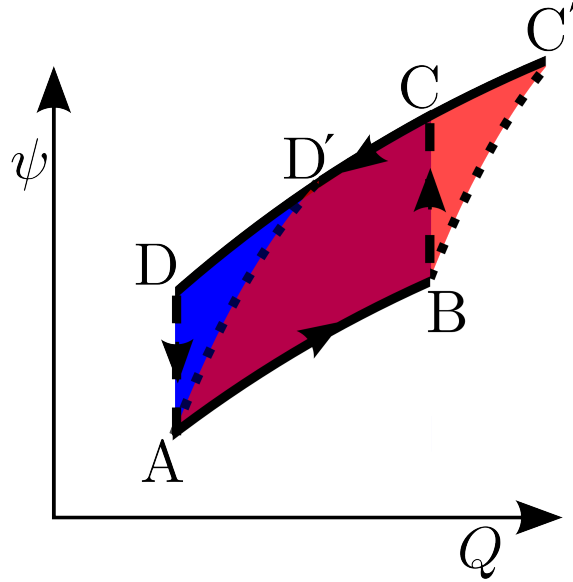

Figure 2: The blue ABCDA-cycle, proposed by Brogioli. And the red ABC'D'A-cycle, proposed by Boon and Van Roij. Both cycle are in the ψ-Q representation and are counterclockwise.

The cycle consists of four steps. In step AB the electrodes are in salt water, the potential increases and the charge builds up. In the next step (BC) the electrodes are disconnected from the voltage source and they are flushed with fresh water. The potential increases because the screening is less for fresh water then for salt water. Then the electrodes are discharged (CD) in fresh water and the potential decreases because of the decrease in charge. In the last step (DA) the system is flushed with salt water. The potential decreases due to the higher screening of salt water. The enclosed (blue) area equals the work obtained from one cycle.

The engine from Brogioli [4] looks a lot like the Stirling heat engine, but this Stirling engine is not the most efficient heat engine. The most efficient heat engine is the Carnot engine. Boon and Van Roij [5] described a new cycle that can be mapped onto the Carnot cycle. The cycle of this engine is also in shown Fig. 2, where it is the ABC'D'A-cycle. This Carnot capacitive mixing cycle differs in two steps from the Brogioli-Stirling engine: BC' and D'A. The third step (C'D') looks different, but is only shifted and is also discharging at fixed concentration (ρ_{L}). In the two other steps the supply of salt and fresh water is cut off during (dis)charging. These canonical steps (fixed number of ions) cause for the bulk concentration (ρ_s) to change from one salinity to another, by either extracting ions from the solution (BC) or releasing them (DA).

Both articles only describe the statics of this system. My predecessor, Kempkes [11], already put some effort into describing the dynamics, but he concluded that his 1D model of planar electrodes could not represent the porous carbon electrodes properly.

2.2 Poisson-Nernst-Planck Equation

The first equation that will be discussed is the Poisson equation. This equation relates the charge distribution in a system to the potential. In this case, the changes in concentration of positive and negative ions play the role of charges. In the electrolyte of the engine the Poisson equation is

$$\nabla^2\phi = -4\pi\lambda_{\mathrm{B}}(\rho_+ - \rho_-). \tag{1}$$

In this case $\phi = \frac{e\psi}{k_{\mathrm{B}}T}$ is the dimensionless potential, with ψ the potential, $\lambda_{\mathrm{B}} = \frac{e^2}{4\pi\epsilon_0\epsilon k_{\mathrm{B}}T}$ the Bjerrum length, with ϵ_0 the permittivity in vacuum and ϵ the relative permittivity of water, e the electron charge, k_{B} the Boltzmann constant and T the temperature in Kelvin. The concentrations of the positive and negative particles are ρ_+ and ρ_- respectively. This Poisson equation holds only inside the electrolyte, because there are no other sources of charge. On the other hand on the surface of the electrode there is an additional term for the charge, $-4\pi\lambda_{\mathrm{B}}\delta(\vec{r} - \vec{r}_{\mathrm{surf}})\sigma$ (σ surface charge density). Note that the Poisson equation is an electrostatic equation, which causes no problems because the speed of the moving charges is much lower than the speed of light, so magnetic effects and retarded potentials can be neglected. Thus the system is electrically static.
The dynamics come in by the equations for the concentration distribution. The Nernst-Planck equation describe the relation of the potential and concentration with the change in concentration:

$$\vec{J}_\pm = -D(\nabla\rho_\pm \pm \rho_\pm\nabla\phi), \tag{2}$$

$$\frac{\partial\rho_\pm}{\partial t} = -\nabla\cdot\vec{J}_\pm. \tag{3}$$

Here $\vec{J}_\pm$ are the fluxes of the ions, D is the diffusion coefficient, $D = \frac{1}{6\pi\beta\eta a}$, with $\beta = \frac{1}{k_{\mathrm{B}}T}$, η is the viscosity in water and a the radius of the particle. For simplicity, in all the models D will be the same for both ions (Na^+ and Cl^-), though $\frac{D_{\mathrm{Cl}^-}}{D_{\mathrm{Na}^+}} = 1.5$ [12]. In the 2D system it saves a lot of computational effort to assume there is antisymmetry between the two electrodes, which requires $D_{\mathrm{Cl}^-} = D_{\mathrm{Na}^+}$.
These five Eq. (1), (2), (3) have five unknowns (ϕ, ρ_+, ρ_-, $\vec{J}_+$ and $\vec{J}_-$) so with the right boundary conditions this is a closed set of equations. Note that the ions are assumed to be point particles and including particle size would require Modified Poisson and Modified Nernst-Planck equations or Dynamical Density Functional Theory (DDFT).

2.3 Poisson-Boltzmann equation and the Gouy-Chapman model

Even though this Thesis focusses on the dynamics the blue engine, at first it is good to take a look at the stationary/equilibrium equations, because it helps developing the more complex models. In equilibrium the time derivative of all quantities is 0. Hence Eq. (3) becomes $\nabla\cdot J_\pm = 0$. On the walls the flux is 0, so Eq. (3) even reduces to $J_\pm = 0$. Equation (2) then becomes $\nabla\rho_\pm = \mp\rho_\pm\nabla\phi$. Which returns the Boltzmann equation for point-like ions in a solvent with boundary condition $\rho_\pm(\phi = 0) = \rho_s$:

$$\rho_\pm = \pm\rho_s e^{\mp\phi} \tag{4}$$

In this equation (and throughout the whole Thesis) ρ_s is the bulk density of the ions. Combining Eq. (1) and (4), the one equation for ϕ in the stationary state is:

$$\nabla^2\phi = -4\pi\lambda_{\mathrm{B}}\rho_s\left(e^{-\phi} - e^{+\phi}\right) = \kappa^2\sinh(\phi) \tag{5}$$

The constant $\kappa^{-1} = \frac{1}{\sqrt{8\pi\lambda_{\mathrm{B}}\rho_s}}$ introduced in this equation is called the Debye length, the typical length for decay of the potential.

In one dimension the Poisson equation can be solved analytically in the stationary case. This solution is called the Gouy-Chapman model (GC). Consider a potential on a plate (dimensionless

potential ϕ_0) at $z = 0$, with a salt solution for $z > 0$.

In the one-dimensional stationary state Eq. (5) becomes $\frac{\partial^2 \phi}{\partial z^2} = \kappa^2 \sinh(\phi(z))$. This second order differential equation requires two boundary conditions. Under the assumption that the potential vanishes far from the plate the first condition is $\phi(z \to \infty) = 0$. The second equation is simply the potential on the wall $\phi(0) = \phi_0$. This leads to the following set of equations for $z > 0$:

$$
\begin{aligned}
\frac{\partial^2 \phi}{\partial z^2} &= \kappa^2 \sinh(\phi(z)) \\
\phi(z \to \infty) &= 0 \\
\phi(0) &= \phi_0
\end{aligned}
$$

In Appendix A the following solution is derived for ϕ:

$$
\phi(z) = 4 \operatorname{arctanh}\left(\gamma e^{-\kappa z}\right) \tag{6}
$$

with $\gamma = \tanh\left(\frac{\phi_0}{4}\right)$. This results shows that κ^{-1} is the length over which the potential decays to zero. With $\lambda_B = 0.72$ nm for water, for salt water with a salt concentration of $\rho_H = 0.6$ M, the Debye length is $\kappa^{-1} = 0.39$ nm. For fresh water with a salt concentration of $\rho_L = 0.024$ M, the Debye length is $\kappa^{-1} = 2.0$ nm. Where M=mol L^{-1} and equal to $6.022 \cdot 10^{23}$ L^{-1} or 0.6022 nm^{-3}.

3   Model

The GC description is excellent for non-dynamical purposes. For the dynamical model that is required for this system it is not useful. First the 1D model will be addressed, because this is an intermediate step to solving the 2D case. Both the 1D and 2D models use the same numerical scheme, further explained in Section 3.2.2 and Appendix C. In the model a few assumptions have been made, the first one has been mentioned above:

- The diffusion coefficient is the same for the positive (Na$^+$) and negative (Cl$^-$) particles.

- The temperature is constant in the whole system and equals the room temperature ($T = 298$ K).

- No chemical/redox reaction occurs on the electrodes.

3.1   1D model

First the one-dimensional system has been solved as an intermediate step, to verify the numerical scheme for this system. This in spite of the fact that the one-dimensional model cannot be used to answer the question posed in this thesis as my predecessor showed [11]. Great advantage of the one-dimensional model is that it can be verified with analytical results of the GC. The system for the one-dimensional model contains two oppositely charged plates ($\phi(\text{plate}) = \pm \phi_0$) at a distance $L = 20\kappa^{-1}$ from each other with dimensionless potential $\phi_0 = 2$. In this case $\kappa^{-1} = \sqrt{8\pi \rho_s \lambda_B}^{-1} \approx 3$ nm, since $\lambda_B = 0.72$ nm and the bulk ion concentration $\rho_s = 0.01$ M (mol L^{-1}). The diffusion coefficient is $D = 1.1 \cdot 10^9$ nm^{2}s^{-1}. The numerical scheme for this model is explained in Appendix C. The solutions to this model together with the analytical solution following from the GC are shown in Fig. 3. The time $\tau = \frac{1}{\kappa^2 D}$ is a typical time for the system, the time it takes for ions to travel over κ^{-1}, since the typical velocity of the ions is $\frac{1}{\kappa D}$. For large t the model and the analytical stationary solution are in excellent agreement, so the computer code works fine in one dimension.

Note that the GC from Section 2.3 was the solution for one charged plate with a half space with salt concentration. In Fig. 3 the GC solution is for oppositely charged plates is shown. This can be done because for either plate the center line between them is practically at infinity. The solution of the GC then becomes

$$\phi_{GC} = -4\operatorname{arctanh}\left(\tanh\left(\frac{1}{2}\right)e^{-(\kappa z + L/2)}\right) + 4\operatorname{arctanh}\left(\tanh\left(\frac{1}{2}\right)e^{+(\kappa z - L/2)}\right) \tag{7}$$
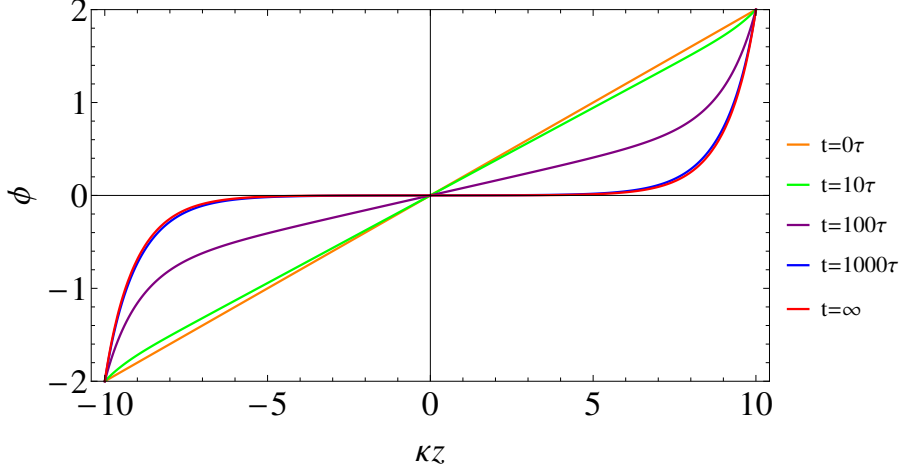
Figure 3: GC compared to the 1D model. The red line is the GC, where the system is in equilibrium ($t = \infty$). The other lines are solution derived from the model for $t = 0\tau$ (Orange), 10τ (Green), 100τ (Purple), 1000τ (Blue).

3.2   2D model

The 1D model is very simple and effective for oppositely charged plates. Unfortunately the blue engine is not just two oppositely charged electrodes. Both electrodes are porous (see Fig. 1), which makes the dynamics much more complicated. Therefore the system that will be investigated in this part contains one pore with a reservoir attached to it.

3.2.1   Geometry

In Fig. 4 the geometry of the system with reservoir attached to a pore is displayed in 2D and 3D. The system has two different kinds of electrodes, one with a positive potential (ψ_0) and one with a negative potential ($-\psi_0$). The one with the positive potential will be modeled and, because of antisymmetry, results apply to the whole system. The 2D geometry will be used in the model, the 3D image is to clarify the 2D model. In Fig. 4a boundary conditions for the potential and the ion concentrations are also given. The dotted line on top of the reservoir is expected to be so far away that this can be considered as the bulk, where $\psi = 0$ and $\rho_\pm = \rho_s$. The electrode is attached to the positive potential, so the potential in the electrode is ψ_0, therefore also the potential on the edge of the electrode is ψ_0. The electrode is rigid so there is no flux through the electrode, hence $\vec{J}_\pm = 0$ in the electrodes.

Figure 4a also gives a boundary condition for the potential and the concentrations on the dashed lines. These lines are symmetry lines, so $\vec{\nabla}\psi \cdot \hat{n} = 0$ and $\vec{J}_\pm \cdot \hat{n} = 0$, so there is no electrical and particle flux through this surface. This is not obvious at first. These conditions follows from looking at multiple pores. Figure 5 shows several pores like the one in Fig. 4a next to each other. This is very schematic and assumes all pores are of the same size and are equally distributed. For
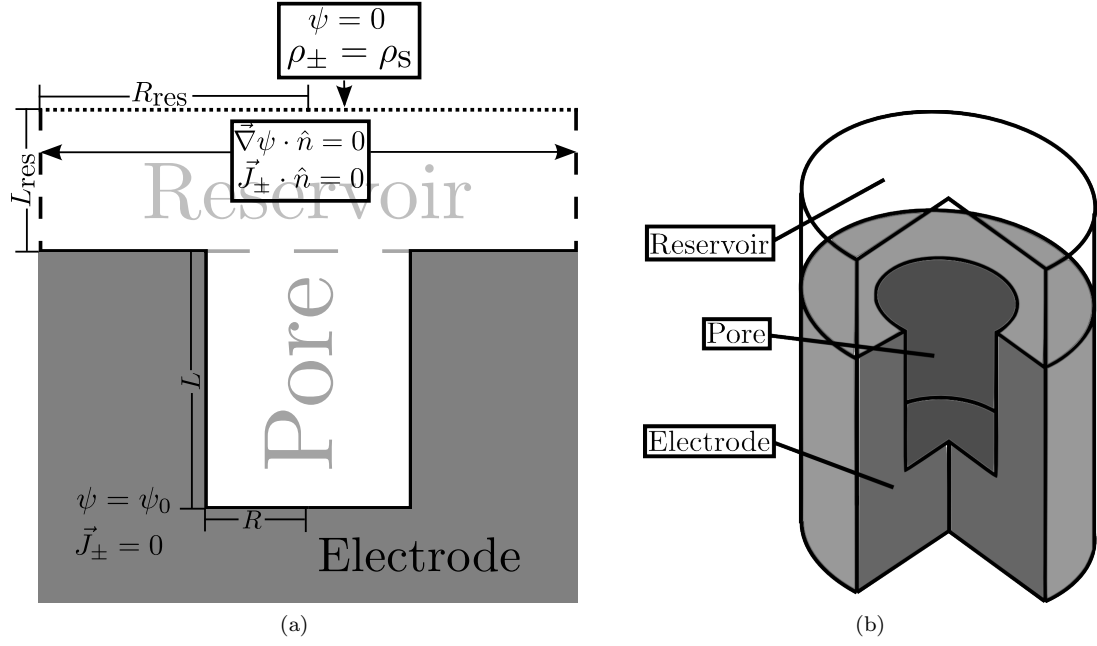
Figure 4: (a) The geometry of system with reservoir attached to pore, with the boundary conditions in the electrode, far away from the pore an at the symmetry lines. (b) Three-dimensional display of the pore-reservoir system.

one pore this can be seen as a average approximation for all the other pores. This becomes very useful in the model. Symmetry on the dashed lines then gives that all the physical quantities have a vanishing spatial derivative perpendicular to this line, which means that $\vec{\nabla}\psi \cdot \hat{n} = 0$ and $\vec{\nabla}\rho_\pm \cdot \hat{n} = 0$. Therefore also $\vec{J}_\pm \cdot \hat{n} = -D(\vec{\nabla}\rho_\pm \pm \rho_\pm \vec{\nabla}\psi) \cdot \hat{n} = 0$.

Beside the boundary conditions, the sizes of the system are also denoted in in Fig. 4a. Because the electrode is microporous, the width of a pore (R) is 1.5 nm and this represents approximately the average micro- and mesopore size. Furthermore half of the volume is occupied by the pores [8], so one can argue that together with Fig. 5, the radius of the reservoir (R_{res}) should be twice the radius of the pore: 3 nm. The length of the pores is a little more difficult, because it strongly depends on the thickness of the electrode. The model uses an equidistant grid, so to be able to model the double layers the distance between two points in direction of the length of the pore cannot be to large. This would give to large numerical errors. On the other hand to restrain the
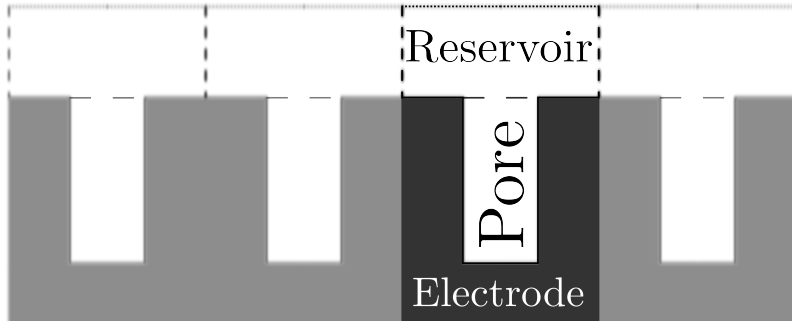
Figure 5: Multiple equal pores next to each other, showing the symmetry of physical quantities at the dashed lines.

calculation time, the number of points has to be small enough. This restricts the length of the pore (L) to 20 nm. The length of the reservoir (L_{res}) is half the length of the pore, so 10 nm. This is because of two reasons. First, for the same reason as for L, to shorten calculation time. Second, the concentrations $\rho_\pm$ are close to ρ_s at such a short range, i.e. the reservoir quickly becomes part of the bulk solution and modeling part of the bulk is not necessary.

3.2.2 Numerical scheme

This section is an overview of the scheme with little mathematical support. Its main objective is explaining the numerical scheme. For more details see Appendix C.

The focus will be on the 2D model, which describes the pore reservoir system. Because the pores are rotationally symmetric, the rotation dependence (θ) drops out of all equations and two dimensions suffice for modeling the system. The 1D system is very similar, only simpler, because the matrices become vectors etc.

The first step is discretising the volume of the geometry. This discretisation is a equidistant grid in both directions, i.e. the spacing between two grid points is constant in both directions. In fact the model has two grids, one grid for the scalars ($\rho_\pm$, ϕ) and one grid for the vectors $J_\pm$. Figure 6 shows both grids. A grid point of the vectors is in the middle of two grid points of the scalars in both directions. So the vector grid points are in the middle of every rectangle of grid points of the scalar and visa versa. This choice of alternating grid and the appropriate numerical scheme ensures particle conservation if the system is closed, which is desired (see Appendix B).

After discretising, all the parameters turn into vectors, with the values at all the points as coordinates. The ∇^2 operator can be discretised and Eq. (1) becomes a matrix equation

$$M\vec{\phi} = rhs$$

This right hand side (rhs) is a vector with mostly $-4\pi(\rho_+ - \rho_-)$, some entries are different depending on boundary conditions. For further explanation of rhs and details of the following see Appendix C. By solving this matrix equation, the dimensionless potential (ϕ) comes out for certain concentration distributions. With this ϕ, the particle fluxes $J_\pm = -D\left(\nabla\rho_\pm \pm \rho_\pm\nabla\phi\right)$ are calculated with the discretised equation. The last step is to calculate the new concentration distribution using the Euler forward method:

$$\rho_\pm(t + \Delta t) = \rho_\pm(t) - \Delta t\vec{\nabla} \cdot \vec{J}_\pm, \tag{8}$$

which is a discrete version of Eq. (3).
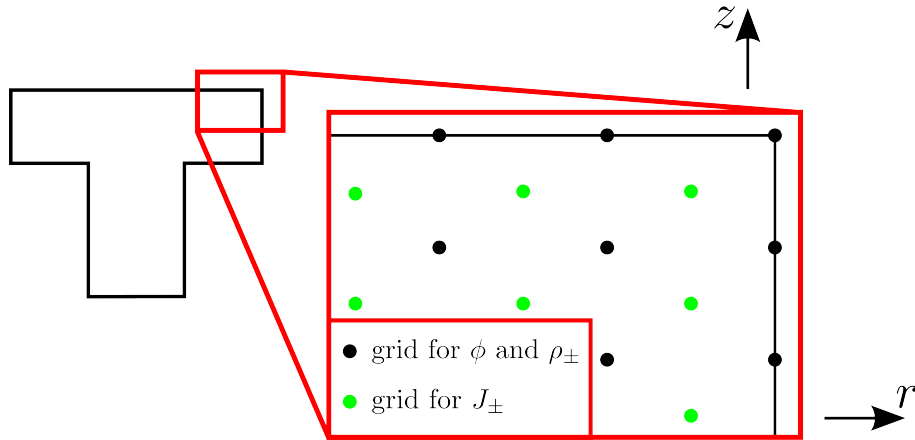
Figure 6: The grid for the scalars (ϕ and $\rho_\pm$) in black and the grid for vectors ($J_\pm$) in green.

3.2.3 Cycle

This section will consider a cycle similar to the cycle Brogioli proposed. The Brogioli cycle is easier to model than the one Boon and Van Roij proposed, because the canonical steps of the latter give more instabilities in the model. The Brogioli cycle consists of four steps. The two flushing steps are not modeled, because that requires hydrodynamics and is beyond the present scope. In fact they can be assumed to happen instantly, since the flushing happens much quicker than the charging and discharging. Therefore only the two grand canonical charging (at $\rho_s = \rho_H$) and discharging (at $\rho_s = \rho_L$) steps will be modeled. The upper left part of Fig. 7 schematically shows the Brogioli cycle. It also shows the whole curves (black) that belong to the ϕ-Q relation for an electrode at a high (ρ_H) and low (ρ_L) salt concentration in equilibrium. From these curves the cycle is constructed by connecting these lines with the dashes black lines. So the ABCDA-cycle along these curves represents the equilibrium cycle, with charging (AB) and discharging (CD) grand canonically and flushing with a fresh water (ρ_L) at high charge (BC) and flushing with salt water (ρ_H) at low charge (DA). Note that the enclosed area is equal to the work per cycle. The lower picture represents what is expected when the charging (AB) and discharging (CD) steps are not done in equilibrium but in a finite time. In this figure red curve is fastest, blue is the slowest and green is the intermediate charging. Hence it is expected that the enclosed area and therefore the work per cycle shrinks. If the charging is too fast the curves might even cross and the cycle will cost energy. On the other hand, the time per cycle also decreases, for some finite charging time.
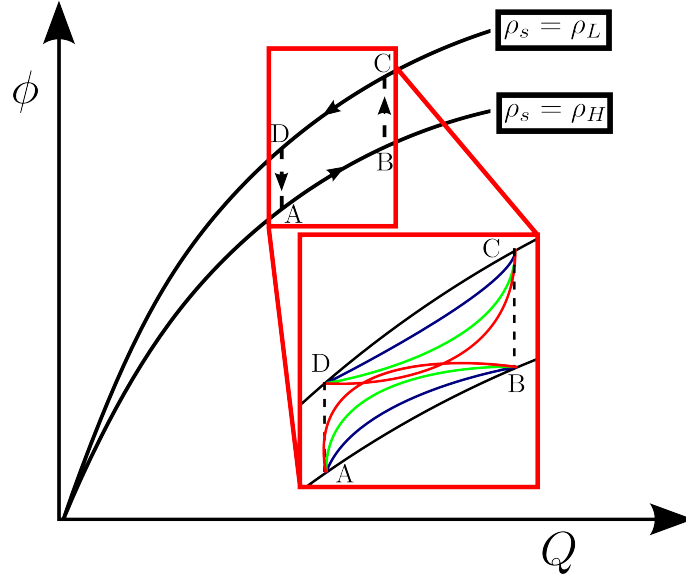
Figure 7: Schematic overview of the Brogioli cycle. The black curves are the equilibrium for charging at high and discharging low concentration. The red, green and blue curve are the dynamical charging and discharging curves.

In the model the potential will be changed over time, the charge follows the potential. The start and end potential for the charging and discharging determine the cycle. Since this model does not take the particle size into account, the concentration of the negative ions at the electrode could rise to undesirably high values. Hence the potential ϕ_0 should not be too high. It is safe to say that the concentration should stay below 10 M. The maximal **bulk** saturation of NaCl in water at room temperature is 360 g L^{-1} or 7 M [16], so in this pore the concentration should definitely stay below 10 M.

In the equilibrium state the system is maximally adjusted, therefore this gives a maximal value

for the negative ion concentration at the (positive) electrode. In equilibrium the concentrations satisfy the Boltzmann equation, so $\rho_- = \rho_{\rm s} e^{\phi_0}$. This gives a constraint on the maximal potential at the electrode:

$$\phi_0 = \log\left(\frac{10}{[\rho_{\rm s}]}\right), \tag{9}$$

with $[\rho_{\rm s}]$ in M. For salt water ($\rho_{\rm s} = 0.6$ M) ϕ_0 can get up to 3. For fresh water ($\rho_{\rm s} = 0.024$ M) the maximal allowed ϕ is 6.

4   Results

At first the equilibrium relation between charge and potential is constructed. From these relations the potentials and charges at the four points of the cycle (ABCD) can be determined. Then the process can speed up and finite-time cycles are calculated. From now on the potential on the electrode is ϕ in stead of ϕ_0 for notational convenience.

4.1   Equilibrium

The first step is to calculate the charge for a range of ϕ for both salinities. In practice it turns out that this model is not suitable for the calculation of the equilibrium at different ϕ, because it is using a dynamical route towards equilibrium. The system starts out at $\phi = 0$ and then ϕ is increased with a step function. The system is considered to be in equilibrium when the flux into the pore is below a certain value. The time to reach equilibrium is called the relaxation time. This relaxation time is plotted in Fig. 8 for several consecutive potentials ϕ for the equilibrium calculation at $\rho_{\rm s} = \rho_{\rm L}$. The fit through these points ($1.1e^{0.64\phi} - 1.1$) shows that this model is not suitable for equilibrium purposes, since the calculation time per point increases exponentially and the calculation up to $\phi = 4$ already takes over a day. For this reason the equilibrium charge-potential relation has only been determined up to $\phi = 4$.

Figure 8: The relaxation times for the system ($\rho_{\rm s} = \rho_{\rm L}$) as a function of ϕ. The potential is increased with 0.25 e.g. from 3.00 to 3.25. The time before relaxation is the time after the system is adjusted to the new potential.
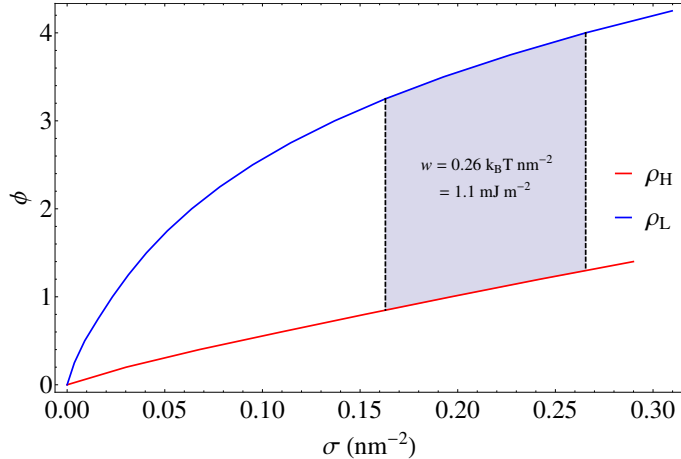
Figure 9: The charge number density (σ) potential (ϕ) relation for $\rho_\mathrm{H} = 0.6$ M and $\rho_\mathrm{L} = 0.024$ M. The dashed lines are the flushing steps and close of the system. The work per unit area per cycle is $0.026\ k_\mathrm{B}T\ \mathrm{nm}^{-2} = 1.1$ mJ m^{-2}.
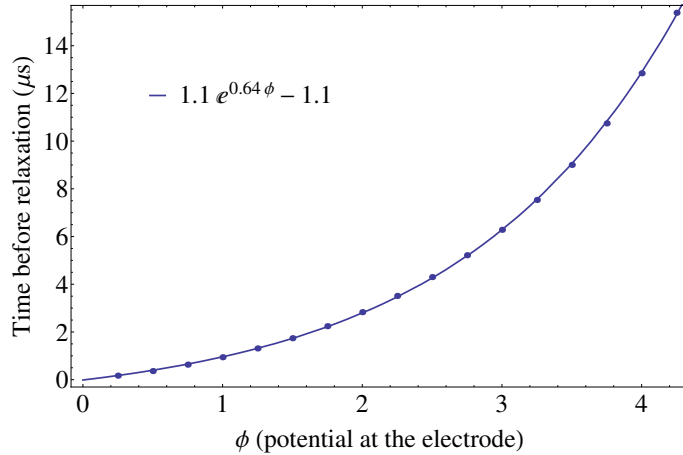
Figure 9 shows the numerical results for this equilibrium charging, where $\sigma = Q/A$ is the number charge (Q) per unit area of electrode (A). The work (W) obtained from the cycle is $\int e\,dQ\,\psi$, because Q is the number charge. In other words $W = k_\mathrm{B}T \int dQ\, \frac{e\psi}{k_\mathrm{B}T} = k_\mathrm{B}T \int dQ\,\phi$ (recall that $\phi = \frac{e\psi}{k_\mathrm{B}T}$). Hence the work per unit area is $w = k_\mathrm{B}T \int d\sigma\,\phi$, is the area of the enclosed surface (blue surface in Fig. 9) multiplied by $k_\mathrm{B}T$. This gives a work per unit area of 1.1 mJ m^{-2} or $0.27\ k_\mathrm{B}T$ nm^{-2}. The surface area per gram electrode is approximately 10^3 m^{2}g^{-1} and the pore volume per gram electrode is 10^{-3} Lg^{-1} [8]. Under the assumption that half of the water flows through the pore, the harvested energy per liter of fresh water is 2 kJ L^{-1} (1 kJ L^{-1} per liter water, salt+fresh). This corresponds approximately to Brogioli's [4] estimate for energy per liter of fresh water of 1.6 kJ L^{-1} and Pattle's [1] guess of 2 kJ L^{-1}.

4.2   Dynamics

As suggested in Fig. 7 the dynamical solutions for the high and the low concentration have the same start and end point as the equilibrium solution of Fig. 9. Reaching the end point would in fact take infinitely long, so the dynamics end points do not really coincide with the equilibrium end points. The potential is gradually increased (or decreased) until 99% of the gain (or the loss) of charge for the equilibrium solution is reached. The potential is increased using a hyperbolic tangent. The charging occurs with ϕ_charging and the discharging with $\phi_\mathrm{discharging}$.

$$\phi_\mathrm{charging} = \phi_\mathrm{A} + (\phi_\mathrm{B} - \phi_\mathrm{A}) \tanh\left(5\frac{t}{t_{\Delta\phi}}\right) \tag{10}$$

$$\phi_\mathrm{discharging} = \phi_\mathrm{C} + (\phi_\mathrm{D} - \phi_\mathrm{C}) \tanh\left(5\frac{t}{t_{\Delta\phi}}\right) \tag{11}$$

Here ϕ_i ($i = \mathrm{A, B, C, D}$) is the imposed electrode potential at state point i in the equilibrium solution. Note that $\phi_\mathrm{B} > \phi_\mathrm{A}$ and $\phi_\mathrm{D} < \phi_\mathrm{C}$, so ϕ_charging and $\phi_\mathrm{discharging}$ indeed have the right sign. The time $t_{\Delta\phi}$ is the transition time which determines the speed of the charging and discharging. In this case the transition time is the same for charging and discharging. At $t = t_{\Delta\phi}$ the 99.99% of the potential difference is bridged, so the end potential is practically on the electrode. This time (or twice this time) is different from the time for one cycle. The time for one cycle contains the whole time for the system to reach the (quasi-)equilibrium endpoints. This time is generally longer then $t_{\Delta\phi}$, because the system needs to relax (ionic charge needs to follow) after the (non quasi-equilibrium) change in potential. In points A and C the system starts from the equilibrium

position. This is not entirely accurate, but since the flushing cannot be calculated with this model, starting from equilibrium is the best option.

In this work only small $t_{\Delta\phi}$ will be investigated, smaller than 1 μs. This is for two reasons. First of all, the system size is small, probably much smaller than in an experiment, where the pores are of the order of the thickness of the electrode (242 μm see, Ref. [14]). If $t_{\Delta\phi}$ is too large the system would constantly be in quasi-equilibrium, which is not an interesting dynamics regime. The second reason is, that the enclosed surface area of the cycle can never become very small, because $\phi_D > \phi_B$. The charging and discharging curves can never cross and the difference is at least $\phi_D - \phi_B$. It turned out that therefore a maximum might only appear for small $t_{\Delta\phi}$ [15]. The cycle is modeled for $t_{\Delta\phi} = 0$ ns, 84 ns, 168 ns, 252 ns, 420 ns, 840 ns. These values might seem odd, since they are not nice decades or centuries. This is because they are actually $0\tau, 10\tau, 20\tau, 30\tau, 50\tau, 100\tau$, where $\tau = 8.4$ ns. This $\tau = \frac{1}{\kappa^2 D}$ is not for either the high or low salt concentrations used in these cycles, but it is a residue of an earlier stage of the model and cannot be overcome anymore at this stage. It belongs to $\rho_s = 0.01$ M.

4.2.1 Time dependence of the surface charge per unit area and the potential and dynamical Brogioli cycles
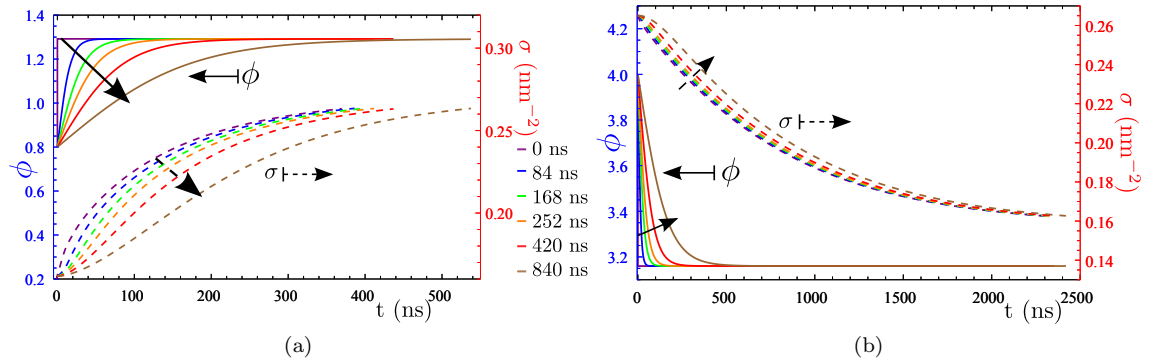
Figure 10: Potential (ϕ solid lines) and surface charge (σ dashed lines) for charging at $\rho_H = 0.6$ M (a) and discharging for $\rho_L = 0.024$ M (b) and for several different transition times: $t_{\Delta\phi} = 0$ ns (Purple), 84 ns (Blue), 168 ns (Green), 252 ns (Orange), 420 ns (Red), 840 ns (Brown). The arrow crossing the graphs points in the direction of increasing $t_{\Delta\phi}$.

Figure 10 shows the time dependence of ϕ (solid) and σ (dashed) for the high ($\rho_H = 0.6$ M, Fig. 10a) and low ($\rho_L = 0.024$ M, 10b) salt concentration. The surface charge density $\sigma = \frac{Q}{A}$ is the total charge on the electrode (Q) divided by the surface area of the electrode (A).
In both cases ϕ is the tanh described as above. These figures show that the electrode charge substantially lacks behind the potential on the electrode. They also show that charging takes much less time (≈ 500 ns) than discharging (≈ 2500 ns). Apparently the system responds much quicker to raising the potential then to lowering. This is caused by the different typical velocities in both cases. As described in the definition of $\tau = \frac{1}{\kappa^2 D}$, the typical velocity of this system is $v_s = \frac{1}{\kappa D} \propto \frac{1}{\sqrt{\rho_s}}$. This gives the ratio $\frac{v_H}{v_L} = \sqrt{\frac{\rho_H}{\rho_L}} = \sqrt{25} = 5$. So discharging in fresh water takes five times as long as charging in salt water. This corresponds to charging and discharging times found in the calculation.

From the results in the two time-dependence plots (Fig. 10) a σ-ϕ-diagram is constructed and shown in Fig. 11. The figure shows the dynamical Brogioli-Stirling cycles for charging and discharging in finite time and the equilibrium result. It clearly demonstrates that the enclosed surface
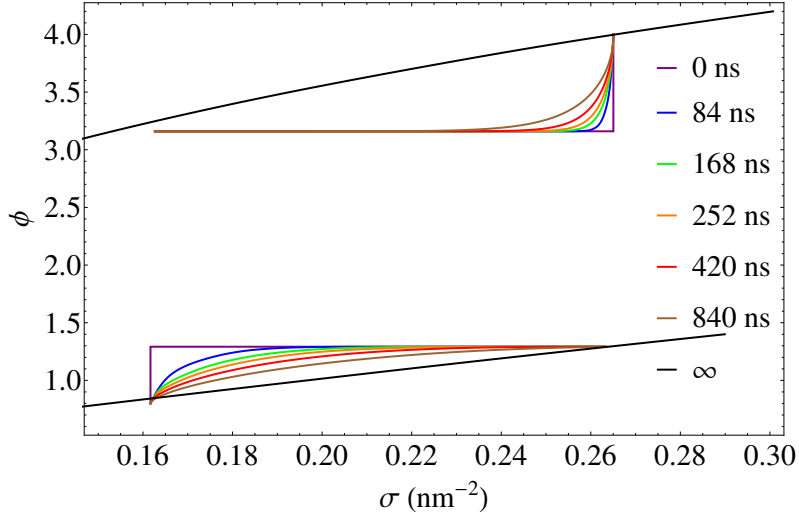
Figure 11: Brogioli-like cycles for dynamical charging and discharging for several different transition times: $t_{\Delta\phi} = 0$ ns (Purple), 84 ns (Blue), 168 ns (Green), 252 ns (Orange), 420 ns (Red), 840 ns (Brown).

area, and therefore the work, decrease with decreasing time. The enclosed area is bounded from below by the enclosed area of the $t_{\Delta\phi} = 0$ solution, which has a positive work. So for every charging and discharging speed work is extracted from this system using this cycle. There is also a slight offset in the beginning of the charging and the end of the discharging. This is probably caused by the way the potentials and equilibrium states where calculated for these points.

4.2.2 Work and power
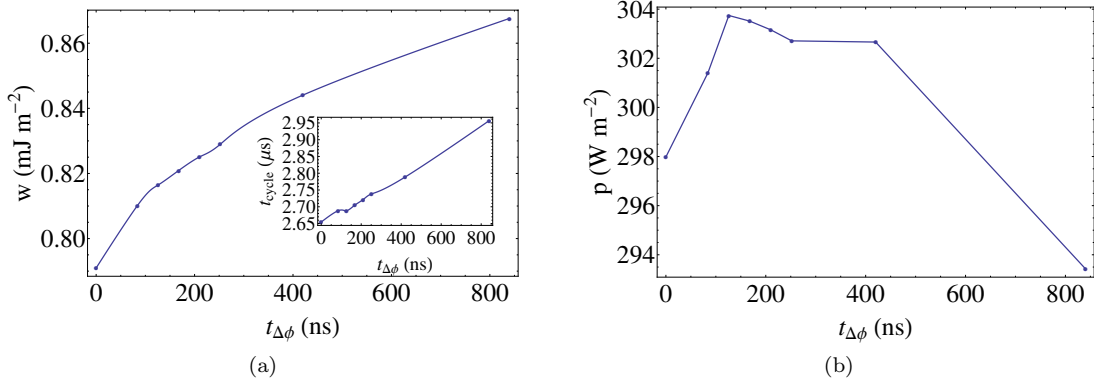
Figure 12: (a) Work per unit area per cycle (w) and in the inset the time per cycle (t_{cycle}) as a function of $t_{\Delta\phi}$. (b) Power output per unit area ($p = \frac{w}{t_{\text{cycle}}}$) a function of $t_{\Delta\phi}$.

As in Section 4.1 the work per unit area of electrode (w) for the dynamical Brogioli-Stirling cycles is the area of the enclosed surface of Fig. 11 in units of $k_{\text{B}}T$ ($= 4.11 \cdot 10^{-21}$ J). In Fig. 12a the work is plotted as a function of $t_{\Delta\phi}$. In order to determine the maximal power output more accurately, two extra calculations were done to find the work at $t_{\Delta\phi} = 126$ ns, 210 ns. The work is clearly decreasing for decreasing $t_{\Delta\phi}$ as one would expect, but also the time per cycle (t_{cycle}) is decreasing

as Fig. 12a also shows in the inset. Combining the two graphs of Fig. 12a gives a power per unit area ($p = \frac{w}{t_{\text{cycle}}}$), which is shown in Fig. 12b. From this figure it is clear that for $t_{\Delta\phi}$ large enough, p decreases to 0. Besides, p is not maximal for $t_{\Delta\phi} = 0$, so because this function is continuous (even C^{∞}) there has to be a maximum for $t_{\Delta\phi} \in]0, \infty[$. It looks like the maximum is somewhere around $t_{\Delta\phi} = 125$ ns with a power output of approximately 304 W m^{-2}. From these results it is not possible to determine where the maximum is exactly. More research should be done to get a better result and understanding of this maximum.

4.2.3 Flushing time

This maximum also depends on the flushing time (t_{flush}). In Fig. 12 and up to now t_{flush} is taken to be 0. Obviously the power output per unit area decreases for all $t_{\Delta\phi}$ when t_{flush} increases, because w stays the same and t_{cycle} increases as t_{flush} increases. What happens to p is less obvious, Fig. 13 shows the movement of the maximum in p for increasing t_{flush}. The work plotted in these graphs $\Delta p = p(t_{\Delta\phi}) - p(t_{\Delta\phi} = 0)$, in order to get all the graphs aligned. The maximum starts to shift to higher $t_{\Delta\phi}$. It is hard to say how much the maximum shift is, but for $t_{\text{flush}} = 1000$ ns the maximum seems to be close to $t_{\Delta\phi} = 400$ ns or higher.
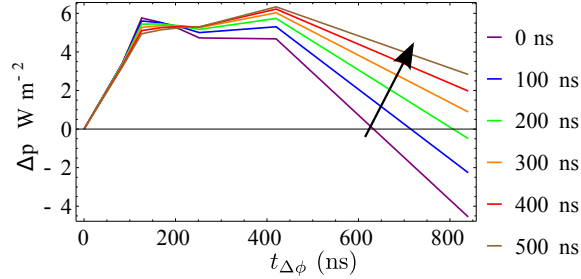
Figure 13: Power output per unit area as a function of $t_{\Delta\phi}$, with $p(t_{\Delta\phi} = 0)$ for several flushing times, $t_{\text{flush}} = 0$ ns (Purple), 100 ns (Blue), 200 ns (Green), 300 ns (Orange), 400 ns (Red), 500 ns (Brown). The arrow points in the direction of increasing $t_{\Delta\phi}$.

5 Conclusion and discussion

A capacitive mixing blue engine harvests work from the increase in entropy that occurs when salt and fresh water mix. A capacitive mixing device consists of porous electrodes, supercapacitor like carbon electrodes, filled with electrolyte (water with positive and negative ions). Brogioli [4] and Boon and Van Roij [5], both described an equilibrium cycle by which this work can be obtained. These equilibrium cycle delivers finite work, but zero power output, because the time per cycle is infinite for equilibrium. Therefore the dynamics of the blue engine were investigated, to find a maximal power output for a blue engine. The electrodes were simplified and assumed to consist of many equal pores attached to a reservoir. One of these pore-reservoir systems was subject of this Thesis.

The dynamics were modeled using the Poisson(1)-Nernst(2)-Planck(3) equation on an equidistant grid by matrix inversion and the Euler forward method. For a cycle similar to the one Brogioli [4] proposed, the work and the power was calculated for several transition times for the potential and for equilibrium for a pore of 20 nm length and 1.5 nm in radius and a reservoir of 10 nm length and 3 nm radius. The flushing steps in this cycle were considered to happen instantaneously. The work per unit area per cycle was much larger for equilibrium (1.1 mJ m^{-2}) than for dynamical cycles ($\sim$0.82 mJ m^2). The equilibrium engine is the most efficient and speeding up the cycle costs energy. But the equilibrium of course did not play a role in maximal power output, because the equilibrium cycles take infinitely long. For transition times around 125 ns, the power output per unit area (p) was maximal. For this transition time p was approximately 304 W m^{-2}. Because of the lack of data points the maximum could not be located more accurately. Also, this maximum is probably not the maximum for a real blue engine system, because the real pores are much longer, so the distance from the reservoir to the end of the pore is longer, hence the charging time is longer. However, the results show that the maximal power output per unit area can be found for a simplification of the blue engine.

On the way some interesting findings came to light. In the dynamical cycles the charging happened a lot quicker than the discharging in the dynamical system. This was due to the fact that the typical velocity scales with $\sqrt{\rho_s}$ and the charging happens in $\rho_H = 0.6$ M and the discharging in $\rho_L = 0.024$ M. It also turned out that the transition time at which the maximal p is found strongly depends on the flushing time (which was considered 0 at first). For $t_{\text{flush}} = 1000$ ns, which is not a long flushing time, the maximum moves to $t_{\Delta\phi} = 400$ ns. Maybe a flushing time of 1000 ns is too large for this system, considering that the time of the cycle is several orders smaller than in a real system due to the short pore and reservoir length.

The equidistant grid forced the system to be small, because the double layer had to be modeled as well, which requires a high grid point density (> 1 nm^{-1}). Implementing a boundary layer or another non-constant grid would make it possible to enlarge the system. Furthermore it would make it possible to get to higher potentials, because these calculations crashed at high potentials ($\phi > 6$). The spacing was not small enough to account for the high values and gradients in ρ_-, which gave instabilities in the numerics and made the model unreliable. This problem can also be solved by taking the particle size into account. This is either by using Modified Poisson-Boltzmann and Modified Nernst-Planck equations or Dynamical Density Functional Theory.(DDFT)

DDFT would also make it possible to implement different ion sizes and therefore different diffusion coefficients. The diffusion coefficient D was taken the same for both ions, but for Na$^+$Cl$^-$ this is not the case and might affect the calculations. Furthermore, the diffusion coefficient used in the model was determined for bulk solution. It is not necessarily true that in such a small compartment, like a pore, this D is the bulk diffusion coefficient, due to frictional or capillary forces.

5.1 Outlook

For further research it would surely be interesting to solve some of the problems above. Some require little effort, like expanding the data set around the maximum, some require a little more, like implementing DDFT. Another interesting follow-up research subject, could be finding a more optimal charging path. As Kooiman [17] proposed charging and discharging path for which the power output is maximal for the oppositely plates model for the Brogioli-Stirling blue engine. She showed that the charging should happen linear in time (constant current, I) and the discharging should follow a certain prescribed relation to ϕ. Even thought this was derived for opposite plates, this may also apply for the pore-reservoir system.

References

[1] Pattle, R E. "Production of Electric Power by Mixing Fresh and Salt Water in the Hydroelectric Pile." *Nature.* **174**, 4431 (1954): 660-660.

[2] Blundell, S., & Blundell, K. M. (2010). *Concepts in thermal physics.* Oxford: Oxford University Press.

[3] Post, J W, J Veerman, H V M Hamelers, G J W Euverink, S J Metz, K Nymeijer, and C J N Buisman. "Salinity-gradient Power: Evaluation of Pressure-Retarded Osmosis and Reverse Electrodialysis." *Journal of Membrane Science.* **288** (2007): 218-230.

[4] Brogioli, D. "Extracting Renewable Energy from a Salinity Difference Using a Capacitor." *Physical Review Letters.* **103**, 5 (2009): 58501.

[5] Boon, N, and R van Roij. "'Blue Energy' from Ion Adsorption and Electrode Charging in Sea and River Water." *Molecular Physics.* **109** (2011): 1229-1241.

[6] Janssen, M, A Härtel, R van Roij, "Boosting capacitive blue-energy and desalination devices with waste heat.", *arXiv:1405.5830v1 [cond-mat.stat-mech].* (2014).

[7] Biesheuvel, P M, S Porada, M Levi, and M Z Bazant. "Attractive Forces in Microporous Carbon Electrodes for Capacitive Deionization." *Journal of Solid State Electrochemistry.* **18**, 5 (2014): 1365-1376.

[8] Kim, T, and J Yoon. "Relationship between Capacitance of Activated Carbon Composite Electrodes Measured at a Low Electrolyte Concentration and Their Desalination Performance in Capacitive Deionization." *Journal of Electroanalytical Chemistry.* **704** (2013): 169-174.

[9] Porada, S, K J Keesman, P M Biesheuvel, M Bryjak, L Borchardt, M Oschatz, S Kaskel, J S Atchison, and V Presser. "Direct Prediction of the Desalination Performance of Porous Carbon Electrodes for Capacitive Deionization." *Energy and Environmental Science.* **6**, 12 (2013): 3700-3712.

[10] Everett, D H, and D H Everett. *Manual of Symbols and Terminology for Physicochemical Quantities and Units: Adopted by the Iupac Council at Washington DC, USA, on 23 July 1971.* London: Butterworths, 1972.

[11] Kempkes, S, "Dynamics of charged particles dissolved in water in an electrolytic cell." Bachelor's Thesis, Institute for Theoretical Physics, Utrecht Univerity. (2014).

[12] Samson, E. "Calculation of Ionic Diffusion Coefficients on the Basis of Migration Test Results." *Materials and Structures.* **36**, 257 (2003): 156-165.

[13] Peskoff, A, and D M Bers. "Electrodiffusion of Ions Approaching the Mouth of a Conducting Membrane Channel." *Biophysical Journal.* **53**, 6 (1988): 863-875.

[14] Porada, S, M Bryjak, der W A van, and P M Biesheuvel. "Effect of Electrode Thickness Variation on Operation of Capacitive Deionization." *Electrochimica Acta.* **75** (2012): 148-156.

[15] Cats, P. "Dynamics of Charging and Discharging Cycles of Blue Energy Devices", Bachelor's Thesis, Fontys University of Applied Sciences (Utrecht Univerity). (2014).

[16] Lide, D R. *CRC Handbook of Chemistry and Physics: A Ready-Reference Book of Chemical and Physical Data.* Boca Raton, FLA: CRC, 2007

[17] Kooiman, M. "Empowering Blue Energy, Ionic responses to external fields and the application of this response to power generators based on capacitive." Master's Thesis, Institute for Theoretical Physics, Utrecht University. (2011).

A Gouy-Chapman model

As described in Section 2.3 the Gouy-Chapman model solves the equilibrium system for a half space $(0 < z < \infty)$ with a potential at $z = 0$. The Poisson equation in one dimension $(\frac{\partial^2 \phi}{\partial z^2}(z) = -4\pi\lambda_B(\rho_+(z) - \rho_-(z)))$ and the Boltzmann equation $(\rho_\pm(z) = \rho_s e^{\mp\phi(z)})$ apply.
These two equations can be combined into:

$$\frac{\partial^2 \phi}{\partial z^2}(z) = \kappa^2 \sinh(\phi(z)) \tag{12}$$

The two boundary conditions are:

$$\phi(0) = \phi_0$$
$$\phi(z \to \infty) = 0$$

Equation (12) can be converted:

$$\frac{\partial^2 \phi}{\partial z^2} = \kappa^2 \sinh(\phi)$$

$$\frac{\partial \phi}{\partial z}\frac{\partial^2 \phi}{\partial z^2} = \frac{\partial \phi}{\partial z}\kappa^2 \sinh(\phi)$$

$$\frac{\partial}{\partial z}\frac{1}{2}\left(\frac{\partial \phi}{\partial z}\right)^2 = \frac{\partial}{\partial z}\kappa^2 \cosh(\phi)$$

So there is a $C \in \mathbb{R}$ such that $\frac{1}{2}\left(\frac{\partial \phi}{\partial z}\right)^2 - \kappa^2 \cosh(\phi) = C$. Since $\lim_{z\to\infty}\phi(z) = \lim_{z\to\infty}\frac{\partial \phi}{\partial z}(z) = 0$, $C = -\kappa^2$. This leads to $\frac{\partial \phi}{\partial z} = \pm\kappa\sqrt{2(\cosh(\phi) - 1)} = \pm 2\kappa\sinh(\frac{\phi}{2})$. The derivative of the potential at the boundary cannot be the same sign as the potential at the boundary, so only the '-' solution is valid. The equation is now $\frac{1}{2\sinh\left(\frac{\phi}{2}\right)}\frac{\partial \phi}{\partial z} = -\kappa$ and:

$$\frac{\partial}{\partial z}\log\left(\tanh\left(\frac{\phi}{4}\right)\right) = \frac{1}{\tanh\left(\frac{\phi}{4}\right)}\frac{1}{4\cosh^2\left(\frac{\phi}{4}\right)}\frac{\partial \phi}{\partial z}$$

$$= \frac{1}{4\cosh\left(\frac{\phi}{4}\right)\sinh\left(\frac{\phi}{4}\right)}\frac{\partial \phi}{\partial z}$$

$$= \frac{1}{2\sinh\left(\frac{\phi}{2}\right)}\frac{\partial \phi}{\partial z}$$

So $\frac{\partial}{\partial z}\log\left(\tanh\left(\frac{\phi}{4}\right)\right) = -\kappa$ or $\phi(z) = 4\operatorname{arctanh}\left(\gamma e^{-\kappa z}\right)$, with γ an integration constant. The other boundary condition gives $\phi_0 = 4\operatorname{arctanh}(\gamma)$, so $\gamma = \tanh\left(\frac{\phi_0}{4}\right)$.

If the system consists of two oppositely charged plates, at some distance L from each other with $L \gg \kappa^{-1}$, then the plates do not affect each others screening and the solutions can be added up.

B Conservation of particles

This appendix provides a prove that numerical scheme described in Section 3.2.2 and Appendix C, ensures particle conservation in a closed system (no particle flux through the boundaries). This scheme uses an alternating grid and the Euler forward method. The two coordinates are x and y discretised by x_i and y_j, with $i = 1, 2, \ldots, n$ and $j = 1, 2, \ldots, m$. For short notation ρ_+ and ρ_- are ρ in this derivation. Conservation of particle means

$$\sum_{i,j} \frac{\partial \rho}{\partial t}\Big|_{i,j} = 0. \tag{13}$$

The Nernst-Planck equations give

$$\frac{\partial \rho}{\partial t}\Big|_{i,j} = -\vec{\nabla} \cdot \vec{J}|_{i,j} = -\left(\frac{\partial J_x^{i,j}}{\partial x} + \frac{\partial J_y^{i,j}}{\partial y} \right). \tag{14}$$

Using the discretisation, the second term of Eq. (14) becomes

$$-\left(\frac{\partial J_x^{i,j}}{\partial x} + \frac{\partial J_y^{i,j}}{\partial y} \right) = -\frac{J_x^{i,j} + J_x^{i,j-1} - J_x^{i-1,j} - J_x^{i-1,j-1}}{\Delta x} - \frac{J_y^{i,j} + J_y^{i-1,j} - J_y^{i,j-1} - J_y^{i-1,j-1}}{\Delta y}. \tag{15}$$

Note that in the summation over i of $-\frac{J_x^{i,j} + J_x^{i,j-1} - J_x^{i-1,j} - J_x^{i-1,j-1}}{\Delta x}$ all terms drop out except for the first and last one, because the next one cancels the one before. Thus only $-\frac{J_x^{n,j} + J_x^{n,j-1} - J_x^{0,j} - J_x^{0,j-1}}{\Delta x}$. Similar for the summation over j, the second term becomes $-\frac{J_y^{i,m} + J_y^{i-1,m} - J_y^{i,0} - J_y^{i-1,0}}{\Delta y}$. For this alternating grid, the grid for J has only $n - 1$ grid points in the x-direction and $m - 1$ grid points in the y-direction. Since the system is closed, all J outside the system are 0. Therefore the following terms vanish:

$$J_x^{n,j} + J_x^{n,j-1} - J_x^{0,j} - J_x^{0,j-1} = 0 \tag{16}$$

$$J_y^{i,m} + J_y^{i-1,m} - J_y^{i,0} - J_y^{i-1,0} = 0 \tag{17}$$

Therefore $\sum_{i,j} \frac{\partial \rho}{\partial t}\big|_{i,j} = 0$, so there is particle conservation for this grid and numerical scheme in a closed system. $\qquad\square$

C Numerical Scheme

Equations (1),(2),(3) are discretised by using $\frac{\partial f}{\partial x}(x_i) = \frac{f(x_{i+1}) - f(x_{i-1})}{2\Delta x}$ and $\frac{\partial^2 f}{\partial x^2}(x_i) = \frac{f(x_{i+1}) - 2f(x_i) + f(x_{i-1})}{\Delta x^2}$. Then the Poisson equation is solved by matrix inversion. From that using equation (2) the flux is calculated. And in the last step the new ρ_+ and ρ_- are determined using (3) for time $t + dt$. Then the cycle repeats.

For the first step the discretisation of comes in. A 1D or 2D geometry can be discretised in one or two coordinates respectively. So therefore the scalar $\phi(\vec{r}, t)$ turns into the vector $\vec{\phi}(t)$. The Poisson equation then becomes a matrix equation $M \cdot \phi = rhs$. In the 1D case this is a tridiagonal matrix and the equation can be solved using the Thomas algorithm. For the 2D case this matrix M turns out to be a tridiagonal block matrix. In order to solve this equation, LU-decomposition is necessary.

C.1 Inversion of a tridiagonal block matrix by LU-decomposition

The general form of this tridiagonal block matrix equation is:

$$Mx = b \tag{18}$$

Where the matrix M looks like

$$
M = \begin{bmatrix}
Y_0 & Z_0 & & & & & \\
X_1 & Y_1 & Z_1 & & & & \\
& X_2 & Y_2 & & Z_2 & & \\
& & \ddots & \ddots & & \ddots & \\
& & & X_{n-1} & Y_{n-1} & Z_{n-1} \\
& & & & X_n & Y_n
\end{bmatrix}
\tag{19}
$$

C.1.1   LU decomposition

LU-decomposition constructs matrices L and U such that $M = LU$, where the matrices L and U are of the form:

$$
L = \begin{bmatrix}
I & & & & & \\
L_1 & I & & & & \\
& L_2 & I & & & \\
& & \ddots & \ddots & & \\
& & & L_{n-1} & I & \\
& & & & L_n & I
\end{bmatrix}
\qquad
U = \begin{bmatrix}
U_0 & Z_0 & & & & \\
& U_1 & Z_1 & & & \\
& & U_2 & Z_2 & & \\
& & & \ddots & \ddots & \\
& & & & U_{n-1} & Z_{n-1} \\
& & & & & U_n
\end{bmatrix}
\tag{20}
$$

It can easily be checked that U_i and L_i $(i = 0, 1, 2, \ldots, n)$ have to be of the following form:

$$U_0 = Y_0$$
$$L_i = X_i U_{i-1}^{-1} = X_i \beta_{i-1}$$
$$U_i = Y_i - L_i Z_{i-1}$$

This definition of β_i will become clear later.

C.1.2   Solving $LUx = b$

Solving this equation requires two steps, first:

$$Ly = b$$

Then:

$$Ux = y$$

First note that $b = (b_0, b_1, \ldots, b_n)$, $y = (y_0, y_1, \ldots, y_n)$, $x = (x_0, x_1, \ldots, x_n)$ are composed of vectors (b_i), (y_i) and (x_i), with dimensions equal to the dimension of the columns of the matrix.

The first few lines of the first equation can now be written as:

$$
\begin{array}{ccccc}
I y_0 & & & = & b_0 \\
L_1 y_0 & + & I y_1 & = & b_1 \\
& L_2 y_1 & + & I y_2 & = & b_2
\end{array}
$$

Hence $y_0 = b_0$ and the other lines give $y_i = b_i - L_i y_{i-1}$.
Now the last few lines of the second equation are:

$$
\begin{array}{ccccc}
& & U_n x_n & = & y_n \\
& U_{n-1} x_{n-1} & + & Z_{n-1} x_n & = & y_{n-1} \\
U_{n-2} x_{n-2} & + & Z_{n-2} x_{n-1} & & = & y_{n-2}
\end{array}
$$

So $x_n = \beta_n y_n$ and $x_i = \beta_i (y_i - Z_i x_{i+1})$.

C.1.3 Calculation before loop

Before the loop starts, the 'inversion' has to be done:

$$\beta_0 = Y_0^{-1}$$
$$L_i = X_i \beta_{i-1}$$
$$\beta_i = (Y_i - L_i Z_{i-1})^{-1}$$

C.1.4 Calculation in the loop

The first step in the loop is:

$$y_0 = b_0$$
$$y_i = b_i - L_i y_{i-1}$$

and the second step:

$$x_n = y_n$$
$$x_i = \beta_i(y_i - Z_i x_{i+1})$$

C.2 Example: Pore with reservoir

The case of Fig. 4(a) will now be further explored. The r direction is discretised by $i = 1, 2, \ldots, n$ and the z direction by $j = 1, 2, \ldots, m$. So we have $\phi_i^j = \phi(r_i, z^j)$ etc.

For notation: $\phi = (\phi_0^1, \phi_1^1, \ldots, \phi_n^1, \phi_0^2, \phi_1^2, \ldots, \phi_n^2, \ldots, \phi_0^m, \phi_1^m, \ldots, \phi_n^m)^{\mathsf{T}}$. Note that $\nabla^2\phi = \frac{\partial^2\phi}{\partial r^2} + \frac{1}{r}\frac{\partial\phi}{\partial r} + \frac{\partial^2\phi}{\partial z^2}$ in cylindrical coordinates. This gives:

$$\nabla^2\phi = \frac{\phi_{i+1}^j - 2\phi_i^j + \phi_{i-1}^j}{\Delta r^2} + \frac{1}{r_i}\frac{\phi_{i+1}^j - \phi_{i-1}^j}{2\Delta r} + \frac{\phi_i^{j+1} - 2\phi_i^j + \phi_i^{j-1}}{\Delta z^2} \tag{21}$$

$$= \phi_{i+1}^j\left(\frac{1}{\Delta r^2} + \frac{1}{2r_i\Delta r}\right) - 2\phi_i^j\left(\frac{1}{\Delta r^2} + \frac{1}{\Delta z^2}\right) + \phi_{i-1}^j\left(\frac{1}{\Delta r^2} - \frac{1}{2r_i\Delta r}\right) + \phi_i^{j+1}\frac{1}{\Delta z^2} + \phi_i^{j-1}\frac{1}{\Delta z^2} \tag{22}$$

$$= a\phi_i^{j-1} + b_i^-\phi_{i-1}^j + c\phi_i^j + b_i^+\phi_{i+1}^j + a\phi_i^{j+1} \tag{23}$$

As said the matrix M is:

$$M = \begin{bmatrix} Y_0 & Z_0 & & & & \\ X_1 & Y_1 & Z_1 & & & \\ & X_2 & Y_2 & & Z_2 & \\ & & \ddots & \ddots & & \ddots & \\ & & & X_{m-1} & Y_{m-1} & Z_{m-1} \\ & & & & X_m & Y_m \end{bmatrix} \tag{24}$$

Inside the reservoirs it is clear that:

$$X_i = Z_i = \begin{bmatrix} 0 & 0 & 0 & 0 & \ldots & 0 \\ 0 & a & 0 & 0 & \ldots & 0 \\ 0 & 0 & a & 0 & \ldots & 0 \\ 0 & 0 & 0 & \ddots & \ddots & 0 \\ \vdots & \vdots & \vdots & \ddots & a & 0 \\ 0 & 0 & 0 & \ldots & 0 & 0 \end{bmatrix} \qquad Y_i = \begin{bmatrix} -1 & 1 & 0 & 0 & 0 & \ldots & 0 \\ b_1^- & c & b_1^+ & 0 & 0 & \ldots & 0 \\ 0 & b_2^- & c & b_2^+ & 0 & \ldots & 0 \\ 0 & 0 & b_3^- & c & \ddots & \ddots & \vdots \\ 0 & 0 & 0 & \ddots & \ddots & \ddots & 0 \\ \vdots & \vdots & \vdots & \ddots & \ddots & c & b_{n-1}^+ \\ 0 & 0 & 0 & \ldots & 0 & -1 & 1 \end{bmatrix} \tag{25}$$

The 1 and -1 in the upper and lower row say that in the rhs the derivative of the potential perpendicular to the wall vanishes. The wall at which $\phi = 0$ is the potential fixed, so $Y_0 = I$ and $Z_0 = 0$. At the height of the pore the X_i and Z_i have no entries inside the electrode. There the potential is determined, so in the electrode $Y_i = I_{\text{electrode}}$. The surface of the electrode belongs also to the inside. The value of the potential is given in rhs. Only on the surface of the electrode $\phi = \phi_0$ and inside it is $\phi = 0$. This does not matter for the calculation, although physically it is expected that $\phi = \phi_0$. This latter would increase storage and run time:

$$
X_i = Z_i =
\begin{bmatrix}
0 & & & & & & & & \\
 & \ddots & & & & & & & \\
 & & 0 & & & & & & \\
 & & & a & & & & & \\
 & & & & \ddots & & & & \\
 & & & & & a & & & \\
 & & & & & & 0 & & \\
 & & & & & & & \ddots & \\
 & & & & & & & & 0
\end{bmatrix}
\qquad
Y_i =
\begin{bmatrix}
1 & & & & & & & & \\
 & \ddots & & & & & & & \\
 & & 1 & & & & & & \\
 & & b_j^- & c & b_j^+ & & & & \\
 & & & \ddots & \ddots & \ddots & & & \\
 & & & & b_k^- & c & b_k^+ & & \\
 & & & & & & 1 & & \\
 & & & & & & & \ddots & \\
 & & & & & & & & 1
\end{bmatrix}
$$

(26)

At the bottom of the pore the potential is specified, because this is also part of the electrode. Therefore $X_m = 0$ and $Y_m = I$ and in the rhs the potential is determined.

So all matrix elements are determined. The only thing one has to be careful about is the elements of the rhs, which are (by construction of M) not all equal to $-4\pi\lambda_{\text{B}}(\rho_+ - \rho_-)$.